

A semi-coherent search strategy for known continuous wave sources in binary systems

C. Messenger*

School of Physics and Astronomy, Cardiff University, Queens Buildings, The Parade, Cardiff, CF24 3AA

(Dated: Wed Aug 3 15:32:27 2011 +0100)

(commitID: aa83996fd7c01dd8636c284a174d657577b169c9)

(LIGO-P1000020-v2)

We present a method for detection of weak continuous signals from sources in binary systems via the incoherent combination of many “short” coherently-analyzed segments. The main focus of the work is on the construction of a metric on the parameter space for such signals for use in matched-filter based searches. The metric is defined using a maximum likelihood detection statistic applied to a binary orbit phase model including eccentricity. We find that this metric can be accurately approximated by its diagonal form in the regime where the segment length is \ll the orbital period. Hence correlations between parameters are effectively removed by the combination of many independent observation. We find that the ability to distinguish signal parameters is independent of the total semi-coherent observation span (for the semi-coherent span \gg the segment length) for all but the orbital angular frequency. Increased template density for this parameter scales linearly with the observation span. We also present two example search schemes. The first uses a re-parameterized phase model upon which we compute the metric on individual short coherently analyzed segments. The second assumes long \gg the orbital period segment lengths from which we again compute the coherent metric and find it to be approximately diagonal. In this latter case we also show that the semi-coherent metric is equal to the coherent metric.

I. INTRODUCTION

The search for continuously radiating sources in binary systems has proven to be a consistently intensive endeavor in a number of branches of astrophysics. The prime focus being the search for pulsars in the fields of Radio and X-ray astronomy, and more recently for non-axisymmetric rapidly rotating neutron-stars in gravitational-wave (GW) astronomy. In the Radio and X-ray fields it has long been known how to perform searches for such systems over relatively short observation times (\ll orbital period), known as “acceleration” searches [1–3]. In this type of search the frequency of a Doppler modulated signal from a source in a binary system is, over the short observation, approximated by its Taylor expansion and the search is performed over a parameter space defined by the frequency and its derivatives. More recent searches, sensitive in the complementary extreme to systems with orbital periods \ll the observation time, have also been successful in the detection of pulsars in the Radio band [4–6]. These searches take advantage of the distinct frequency domain signature generated by a frequency modulated signal such as a Doppler modulated continuously emitting pulsar in a binary system. This type of search is also planned for application to the GW case [7].

In this work we are motivated by the problems inherent to detection of GW radiation from known binary systems, of which primary examples are the low-mass X-ray binaries (LMXBs). In this case the signal is expected to be extremely weak and the parameter space known to be very large, the proverbial “needle in a haystack”. This is also a long standing issue for X-ray astronomy for a subset of these objects [8, 9]. Here we consider known objects as systems where the sky-

position is assumed to be known precisely and that the intrinsic source frequency, as well as the orbital parameters of the system, are unknown. In the search for GWs from such objects, to date, two strategies have been employed, one being a fully coherent analysis [10] spanning only a short observation time, and the other employing a cross-correlation technique [11] using data from multiple detectors. In the former a parameter space covering was used based on the coherent parameter space metric on a non-eccentric phase model with known orbital period [12]. The coherent metric, as we will show in the Section I C, is simply a measure of “distance” defined on the parameter space and informs us on how to place templates (or filters) optimally within the parameter space for a coherent search. Here we aim to expand on this approach and compute the semi-coherent metric, a similar measure of distance but defined on a semi-coherent detection statistic.

The first work on the coherent parameter space metric for sources in binary systems [12] has recently been built upon by [13] where it has been shown for the GW case that searches for the LMXBs are computationally bound meaning that the number of templates one is required to process to optimally cover the parameter space is too large to be computed on human time-scales. The apparently optimal fully-coherent approach is therefore unfeasible. This is a common theme within continuous GW data analysis for large parameter space searches and has been addressed via various applications of what we will call “semi-coherent” searches. This is where an observation is divided into a number of individual coherent observations, or “segments”, which are then incoherently combined to form a more powerful detection statistic. The term “semi-coherent” is in reference to the fact that the unknown phase of the signal has been either maximized or marginalized away within each segment of the analysis and hence there is no required phase coherence between the signal and our phase model for the duration of the entire observation span. Since the number of templates required for fully-coherent searches typically scale with the coherent observation time to a power

*Electronic address: chris.messenger@astro.cf.ac.uk

$l > 1$, by dividing up the observation into M segments the number of templates required to cover all segments (the number for each segment multiplied by the number of segments) will be reduced by a factor of M^{-1} . The missing piece of the puzzle for sources in binary systems is the method by which to combine the detection statistics computed on the templates within each coherently analyzed segment. This is also true in the case of the search for X-ray pulsations from the LMXBs where, in addition to being computationally bound just as in the GW case, single observations of individual sources from X-ray timing satellites such as RXTE (Rossi X-Ray Timing Explorer) are typically restricted to time-scales of order ~ 1 hour. This limitation, due to scheduling constraints and obscuration of the source as the detector orbits the earth, represents an automatic and unavoidable division of the complete dataset into segments.

The work presented here is based on that of [14–16] who were the first to describe the concept of the metric, based on a distance measure equivalent to the expected loss in the detection statistic between signal and template (the mismatch) in a matched-filter based search. From such a metric one would then proceed to place templates within the parameter space based on the criteria that the mismatch at any given point was always less than a desired threshold. In [17] it was shown that the metric on the general semi-coherent detection statistic was simply the average of the coherent metrics from the constituent segments. Recent work by [18, 19] has described the construction of such a metric on the parameter space defined by the frequency and its derivatives and the sky coordinates. This result is specific to all-sky, wide band, searches for GWs from unknown isolated sources. In this work we compute the semi-coherent metric for the complementary class of sources, the known sources with known sky position in binary systems with unknown frequency and orbital parameters.

In the remainder of this section we review the binary system signal model and the power-like detection statistic as well as the coherent and semi-coherent metric definitions. In Section II we describe the calculation of the coherent and semi-coherent metric for the specific case of sources in binary systems. In particular we analyze two complementary scenarios, in Section II A we deal with cases where the segment length is \ll the orbital period of the source and in Section II C the case where the segment length \gg the orbital period. In each case we outline a basic method for the practical implementation of a search, and in Section III we summarize our findings.

A. The signal model

We model a continuously emitting source of radiation (either GW or electromagnetic (EM)) located within a binary system with a non-emitting companion. In this sense we define the noise-free continuous signal received at an inertial reference frame to be

$$s(t) = A \sin [\Phi(t) + \Phi_0] \quad (1)$$

where A is the constant signal amplitude and Φ_0 is a constant phase offset. Note that in the following we are assuming that

the intrinsic source frequency is constant (i.e. there is no *intrinsic* frequency-evolution of the source) and that any detector motion relative to the chosen inertial reference frame has been accounted for. The latter assumption in practice requires that the sky-position of the source is known to high accuracy and that the time-series has been barycentered (usually to the solar-system barycenter). We also ignore the slowly varying amplitude response in the case of a GW signal. The remaining phase contribution is assumed to be entirely due to the constant intrinsic frequency and the Roemer delay across the source orbit.

This time-dependent phase for a source in a bound eccentric (non-relativistic) orbit is [20]

$$\Phi(t) = 2\pi\nu \left\{ t - t_{\text{ref}} + a \left[\sin \omega (\cos E(t) - e) + \cos \omega \sin E(t) \sqrt{1 - e^2} \right] \right\} \quad (2)$$

where ν is the intrinsic signal frequency¹, t_{ref} is some reference time (at which the signal phase is equal to Φ_0 in the source frame), a is the orbital semi-major axis projected along the line of sight and divided by the speed of light, ω is the argument of periaapse, e is the orbital eccentricity and E is the eccentric anomaly. The eccentric anomaly is defined by the transcendental relation

$$\frac{2\pi}{P} (t - t_p) = E - e \sin E \quad (3)$$

where P is the orbital period (equal to $2\pi/\Omega$ where Ω is the orbital angular frequency) and t_p is the time of periaapsis (the point of closest approach to the prime focus of the orbit).

With regards to the search for continuous GW emission from sources in binary systems, the primary targets (as mentioned in Section I) are the LMXBs. These sources are observed to have highly circularized orbits (see [13] for detailed descriptions of current orbital parameter estimates) and as such we have chosen to limit our investigations to low-eccentricity orbits. In the low-eccentricity limit ($e \ll 1$) we can adopt the approximation [21, 22]

$$\Phi(t) \approx 2\pi\nu \left\{ t - t_{\text{ref}} + a \left[\sin \psi(t) + \frac{\kappa}{2} \sin 2\psi(t) - \frac{\eta}{2} \cos 2\psi(t) - \frac{3\eta}{2} \right] \right\}, \quad (4)$$

where we have Taylor-expanded the orbital contribution to the phase in powers of the eccentricity e up to leading order. In addition we have adopted the following parameters,

$$\kappa = e \cos \omega, \quad (5a)$$

$$\eta = e \sin \omega, \quad (5b)$$

¹ We have assumed that the velocity of the binary barycenter is constant relative to the inertial reference frame and hence absorbed any Doppler shifts into ν .

as replacements for the more physical e and ω parameters. This change is motivated by the fact that for low-eccentric systems strong degeneracies between the argument of periape ω and the time of periape passage t_p would complicate our analysis. In addition we also define

$$\psi(t) = \Omega(t - t_{\text{asc}}), \quad (6)$$

as the time dependent orbital phase as measured relative to the time of passage through the ascending node of the orbit $t_{\text{asc}} = t_p - \omega/\Omega$.

The circular orbit case is a specific instance of the more general elliptic orbit (Eq. 2). For $e = 0$ we can write the phase model in this case as

$$\Phi(t) = 2\pi\nu [t - t_{\text{ref}} - a \sin \psi(t)] \quad (7)$$

where the extraneous parameter ω has been set to $\omega = \pi$ such that, just as for the Taylor-expanded low eccentricity case, the orbital reference time is the time of passage through the ascending node of the orbit rather than the, now meaningless, time of periape t_p .

For the majority of our primary sources, the LMXBs, the expected eccentricities in these systems are relatively low (typically $> 10^{-3}$). However, despite the apparent current requirement for circular orbits only, we continue the analysis using the phase defined for a low-eccentricity orbit (Eq. 4) since the results that follow from this choice can easily be interpreted for either the eccentric or circular orbit cases.

B. The detection statistic

In searching for deterministic signals in noisy data one wishes, in general, to distinguish between the noise hypothesis and the signal-plus-noise hypothesis in order to determine the presence of a signal. In this case the likelihood-ratio test is optimal in the Neyman-Pearson sense [23]. If we assume that our measured time-series data-set consists of our signal and additive Gaussian noise sampled uniformly at discrete times t_j such that

$$x(t_j) = s(t_j, \boldsymbol{\theta}') + n(t_j), \quad (8)$$

where $\boldsymbol{\theta}'$ is a vector containing the signal parameters. We can write the likelihood function as

$$L(\boldsymbol{\theta}') \propto \exp \left\{ -\frac{1}{2} \sum_{j=1}^N \sum_{k=1}^N (x_j - s_j(\boldsymbol{\theta}')) C_{jk}^{-1} (x_k - s_k(\boldsymbol{\theta}')) \right\}, \quad (9)$$

where C is the noise covariance matrix, N is the number of samples in our time-series and for simplicity of notation we have replaced $x(t_j)$ with x_j and $s(t_j)$ with s_j .

One can show that twice² the log-likelihood ratio (the log of the ratio between the likelihood function defined above and

the likelihood assuming no signal), when analytically maximized over the “nuisance” parameters A and Φ_0 , becomes

$$\Lambda(\boldsymbol{\theta}) = \frac{4}{S_n \Delta T} \left| \sum_{j=1}^N \Delta t x_j e^{-i\Phi_j(\boldsymbol{\theta})} \right|^2 \quad (10)$$

in the case of “white” noise where the covariance matrix is diagonal³. Note that the un-primed $\boldsymbol{\theta}$ represents the reduced parameter set after having removed the dependence upon the nuisance parameters and that we have used Δt as our sampling time, $\Delta T = N\Delta t$ as our time span and S_n as the single-sided noise spectral density (assumed constant over the frequency band of interest). This detection statistic has the form of a Fourier power with the exception that the complex phase, with which we multiply each datum, contains an orbital phase component in addition to the intrinsic frequency component.

The statistical behavior of the log-likelihood ratio detection statistic in additive Gaussian noise follows that of a χ^2 distribution. In the simplified constant amplitude case described here the random variable $\Lambda(\boldsymbol{\theta})$ is described by a non-central χ^2_2 distribution (the subscript indicates the number of degrees of freedom). Assuming a set of signal parameters $\boldsymbol{\theta}$ the expectation value of $\Lambda(\boldsymbol{\theta})$ evaluated at an offset parameter space location $\boldsymbol{\theta} + \Delta\boldsymbol{\theta}$ is then given by

$$E[\Lambda(\boldsymbol{\theta}, \Delta\boldsymbol{\theta})] = 2 + \rho^2(\boldsymbol{\theta}, \mathbf{0}) \left| \sum_{j=1}^N e^{i\Delta\Phi_j(\boldsymbol{\theta}, \Delta\boldsymbol{\theta})} \right|^2, \quad (11)$$

where $\rho^2(\boldsymbol{\theta}, \mathbf{0})$ is the optimal signal-to-noise ratio (SNR) given by

$$\rho^2(\boldsymbol{\theta}, \mathbf{0}) = \frac{2}{S_n} \sum_{j=1}^N \Delta t s_j^2(\boldsymbol{\theta}). \quad (12)$$

Note that we have used $\Delta\Phi_j(\boldsymbol{\theta}, \Delta\boldsymbol{\theta}) = \Phi_j(\boldsymbol{\theta} + \Delta\boldsymbol{\theta}) - \Phi_j(\boldsymbol{\theta})$ to represent the phase offset caused by the offset in parameter space location. Also note that the second term in Eq. 11 is equal to the non-centrality parameter governing the χ^2_2 distribution which becomes the optimal signal-to-noise-ratio (SNR) squared when the template and signal parameters are exactly matched. In our problem we are faced with a continuum of signal hypotheses defined by the parameter space spanned by $\boldsymbol{\theta}$, which we must somehow sample from. The common frequentist strategy in parameter space searches is to maximize the detection statistic over all unknown parameter values. For two of these parameters, A and Φ_0 , we have performed this maximization analytically. In the following section we describe the standard strategy for performing the remaining maximizations⁴.

² We multiply the log-likelihood ratio by 2 so that it is exactly consistent with a χ^2 distribution with 2 degrees of freedom.

³ This is a valid assumption for practical purposes since analyses are typically divided into narrow frequency regions within which the noise spectral density can be assumed “white”.

⁴ We note that strictly speaking, the optimality of the standard likelihood-

For a deterministically amplitude modulated signal, such as in the GW case, the standard technique is to analytically maximize not only over the phase and amplitude of the signal but also over the inclination angle of the source and the polarization angle of the GW wave [25]. In such a case the detection statistic becomes a χ^2 statistic with 4 degrees of freedom.

C. The coherent metric

The parameter space in our case is defined by the ranges in uncertainty on the frequency and orbital parameters defining our signal. When faced with the prospect of searching this space for the true signal parameters we rely on the concept of the parameter space metric [14–16] which allows us to set a measure of distance by which we can determine how to sample within the space. Using this geometrical approach we are able to satisfy the constraints that our templates will not be placed too coarsely such we will not “miss” a signal and also that they will not be placed too finely such that we will be wasting computational effort. The standard choice is to define the distance measure for a coherent analysis as the ratio of the expectation value of the loss in SNR local to a signal’s true parameters and the expectation value of SNR at the true signal parameters. This measure, or mismatch, is then

$$\mu(\theta, \Delta\theta) = \frac{\rho^2(\theta, \mathbf{0}) - \rho^2(\theta, \Delta\theta)}{\rho^2(\theta, \mathbf{0})}, \quad (13)$$

where we use By Taylor-expanding the mismatch around the true signal location θ we obtain

$$\mu(\theta, \Delta\theta) = g_{\mu\nu}(\theta) \Delta\theta^\mu \Delta\theta^\nu + o(\Delta\theta^3) \quad (14)$$

where the coherent metric $g_{\mu\nu}(\theta)$ is defined as

$$g_{\mu\nu}(\theta) = \left\langle \frac{\partial\Phi(\theta)}{\partial\theta^\mu} \frac{\partial\Phi(\theta)}{\partial\theta^\nu} \right\rangle - \left\langle \frac{\partial\Phi(\theta)}{\partial\theta^\mu} \right\rangle \left\langle \frac{\partial\Phi(\theta)}{\partial\theta^\nu} \right\rangle \quad (15)$$

with $\langle \dots \rangle$ representing the average over the coherent observation time and with $\Delta\theta^\mu$ representing the deviation in the μ ’th parameter from its true value.

D. The semi-coherent metric

The first stage of a semi-coherent analysis is the process of performing the multiple constituent coherent analyses on the M independent data segments into which the full observation has been divided⁵. Such separate analyses will result in the

ratio applies only for the point-hypothesis case. It has been shown [24] that the optimal statistic in the more general case (including the point hypothesis case) where one is faced with a continuum of signal hypotheses (defined one some parameter space) is the Bayesian statistic, the “Bayes Factor”.

⁵ Whilst in this work we concentrate on a division of the complete dataset in the time domain, semi-coherent searches in general may also suit division of the dataset in the frequency domain, e.g. [7].

generation of discretely sampled values of the detection statistic Λ_m on the parameter space spanned by θ , where m indexes the segment number. Note that the metric in each segment and therefore also the mismatch will vary between segments since the metric can be a function of the segment epoch (as is the case in our binary system).

Since Λ_m are maximized log-likelihood ratios it follows that a sensible choice is to define the semi-coherent detection statistic as the sum of these values as a function of θ ,

$$\hat{\Lambda}(\theta) = \sum_{m=1}^M \Lambda_m(\theta). \quad (16)$$

Therefore, such a statistic would itself represent a log-likelihood on the space spanned by θ , with the understanding that there has been an implicit maximization over M distinct amplitudes A_m and $\Phi_{0,m}$.

In practice, the reason behind adopting an semi-coherent strategy is likely that we lack the computational resources required to coherently track the phase of a signal over long observation times. In which case the introduction and maximization of M distinct initial phases is an approximation to the true phase model. We note that the similar introduction of the M distinct signal amplitudes also does not appear to be consistent with our original signal model. The semi-coherent detection statistic is now also sensitive to signals for which the amplitude varies with a time-scale \gg the coherent segment length ΔT . This subtle feature is a potential improvement with regards to searches in the X-ray spectrum for signals from LMXBs where the amplitude is not necessarily expected to be constant [26].

Based on the fact that the individual segment Λ_m values are χ^2 distributed it follows from Eq. 16 that $\hat{\Lambda}$ is χ^2_{2M} distributed with a non-centrality parameter equal to the sum of the individual segment non-centrality parameters. The expectation value of $\hat{\Lambda}(\theta)$ is therefore given by

$$E[\hat{\Lambda}(\theta, \Delta\theta)] = 2M + \sum_{m=1}^M \rho_m^2(\theta, \Delta\theta). \quad (17)$$

The semi-coherent mismatch (defined as the loss in semi-coherently summed SNR) is then

$$\hat{\mu}(\theta, \Delta\theta) = \frac{1}{M} \sum_{m=1}^M \frac{\rho_m^2(\theta, \mathbf{0}) - \rho_m^2(\theta, \Delta\theta)}{\rho_m^2(\theta, \mathbf{0})}, \quad (18a)$$

$$= \frac{1}{M} \sum_{m=1}^M \mu_m(\theta, \Delta\theta), \quad (18b)$$

where we have assumed that each segment has identical duration and noise level. In practice, whilst it may be simple to maintain constant segment lengths, detector noise may vary between segments. In addition, for GW detectors, amplitude modulation of the signal due to the changing response of the detector as the earth rotates will have an effect [27].

By substituting Eq. 14 into Eq. 18b the semi-coherent metric $G_{\mu\nu}(\theta)$ can then be expressed as

$$G_{\mu\nu}(\theta) = \frac{1}{M} \sum_{m=1}^M g_{\mu\nu}^{(m)}(\theta). \quad (19)$$

This is the standard result, as shown in [17], that the semi-coherent metric is simply the element-by-element average of the constituent coherent metrics.

E. Template placement

In both the coherent and semi-coherent stages of the analysis the intention is to use the information contained in the metric description of the parameter space to place templates. The task is then to cover such a space efficiently whilst adhering to the constraint that no template should have mismatch with any potential signal, greater than a given threshold, μ^* . In this work we simply refer the reader to recent efforts made in the field of GW data analysis with regards to metric based template placement⁶.

In the case of a constant metric, one in which either careful parameterization or luck has left a metric of which the elements are constant over the parameter space, the problem is directly equivalent to the “sphere covering” problem [28]. This was realized and investigated, in the context of GW data analysis, in [29]. In general, in the constant metric case the optimal solution (in the sense of guaranteed parameter space coverage) is to use an n -dimensional lattice of templates. The most basic (but inefficient) of these lattices being the hyper-cubic Z_n lattice and the most efficient being the class known as the A_n^* lattice.

For the more general case of a metric whose elements are functions of the location in the space itself, template placement is more difficult. The coordinate volume and orientation of the area local to a template will change as one moves through the parameter space. Hence the density and relative separations between templates in each of the dimensions of the space changes depending on where we are placing templates. An optimal solution to this particular problem has yet to be found although recent work on so-called “random” and “stochastic” template banks [30–33] shows impressive covering performance especially for higher dimensional spaces. These methods use only information regarding the required local template density, a quantity proportional to the square root of the determinant of the metric.

F. Combining results from different segments

Let us imagine that the coherent detection statistic has been computed for all templates in all segments. We now have the information required to compute an ensemble of semi-coherent detection statistics and the general form of the semi-coherent metric (Eq. 19) tells us how to construct a semi-coherent template bank on the same parameter space. We note that the semi-coherent template bank is a) potentially sampled

far more finely than the coherent template banks, and b) potentially defined on a different parameter space coordinate system (this is the case for the scenario described in Section II A). For each semi-coherent template we need to perform the following.

Firstly, for each coherent segment we transform the parameters of the semi-coherent template into the parameters used in the segment. For each set of transformed coordinates we interpolate the value of the detection statistic on the coherent template bank at the desired parameter space location. The interpolated detection statistics are then summed according to Eq. 16. This is repeated for each template in the semi-coherent template bank.

A particularly fast and simple interpolation method is to use the nearest neighbor approach, the speed and simplicity of which benefits from the use of a hyper-cubic lattice within each segment. Higher precision is achieved by using smaller mismatches in the coherent stage. Using both the inefficient hyper-cubic lattice and decreasing the mismatch will of course increase the computational cost of computing the coherent stage of the analysis.

The assumption that the coherent analysis had been computed prior to this procedure need not be the case in practice. One could perform the interpolation and summing as each segment is being analyzed as long as the total time span of the complete data-set was known a priori, since as we will see, the semi-coherent metric is dependent upon the total time span.

II. RESULTS

In this section we report on the results obtained through calculation of the semi-coherent metric elements via Eq. 19 using the binary system phase model given by Eq. 4. In parallel we provide basic schemes for the practical application of a semi-coherent search in two observational regimes determined by the length of the coherent observation ΔT . The first having a “short” coherent stage with $\Delta T \ll P$ where the segment length is far shorter than the orbital period, and the second having a “long” coherent stage $\Delta T \gg P$ where the segment length exceeds the orbital period.

A. The coherent metric for “short” ($\Delta T \ll P$) coherent segments

In practice one need not compute the coherent detection statistic for all segments using templates given by the semi-coherent metric. The semi-coherent metric tells us how finely we must sample the parameter space for the complete semi-coherent analysis. It is the coherent metric that tells us how finely we must sample each segment.

In the “short” segment regime the coherent metric, calculated in our physical frequency and orbital parameter space, develops strong parameter degeneracies for short observation times, making template placement difficult. In this situation the reduction in detection statistic due to offsets between the

⁶ Note that there are many other parameter space exploration strategies that do not use the metric e.g. Markov-Chain-Monte-Carlo methods.

template and the signal in one parameter can be effectively counteracted by offsets in another. Additionally, the coherent metric computed in any chosen coordinates, would in general result in different *physical* parameter template locations in each segment. Therefore, once the coherent segments have been processed, for a given semi-coherent template there will not be a collection of corresponding coherent segment detection statistics to sum together all computed at the exact same parameter space location.

To address the first issue we propose the adoption of a re-parameterization [18] that greatly simplifies the phase model but that is only valid in the limit $\Omega\Delta T \ll 1$, i.e. when the length of coherent segment is only a fraction of the orbital period. In this case, by simple Taylor-expansion of the phase model, given by Eq. 4, in terms of the time t about the midpoint of each coherent observation we obtain an approximate phase model given by

$$\Phi_m(t_j, \mathbf{u}) = \Phi_0^{(m)} + 2\pi \sum_{k=1}^n \frac{u_k^{(m)}}{k!} (t_j - t_{\text{mid}}^{(m)})^k \quad (20)$$

where $t_{\text{mid}}^{(m)}$ is the midpoint of the m 'th segment, $\Phi_0^{(m)}$ is the phase at this midpoint and the new coordinates $u_k^{(m)}$ map to the physical parameters via the equations given in Appendix A. Note that the \mathbf{u} coordinates themselves are exactly the instantaneous phase derivatives at the midpoint of each segment indexed by k which runs from 1 to n . Also note that by this re-parameterization the boundaries of the parameter space in the new coordinates will not have the same shape as the physical parameter boundaries.

By direct application of Eq. 15 to our re-parameterized phase model we find that the metric in the \mathbf{u} coordinates is

$$g_{\mu\nu}(\mathbf{u}) = \begin{cases} \frac{\pi^2 \mu\nu \Delta T^{\mu+\nu}}{2^{\mu+\nu-2} (\mu+1)! (\nu+1)! (\mu+\nu+1)}, & \mu + \nu = \text{even} \\ 0, & \mu + \nu = \text{odd.} \end{cases} \quad (21)$$

Here we see that the elements themselves are independent of parameter space location making this a constant metric and therefore simple for template placement. The fact that the $g_{\mu\nu}(\mathbf{u})$ elements vanish for $\mu + \nu$ being odd indicates a lack of correlation between adjacent phase expansion terms, a feature that is exemplified in Fig. 1. In this figure we show the results of a simulation in which the coherent mismatch $\mu(\mathbf{u}, \Delta\mathbf{u})$ has been computed in a region in the \mathbf{u} parameter space surrounding a simulated noise-free signal. The degree of correlation between the parameters for the cases where $\mu + \nu$ is even is clearly indicated by the diagonal orientation of the mismatch contours. Also evident from the figure is that the predicted 10% mismatch contour, computed using the metric approximation given in Eq. 21, is in good agreement with the simulation results. The metric itself is a quadratic approximation around the peak of the log-likelihood ratio and in general is only expected to be accurate in the regime $\mu \ll 1$. As we move away from the true signal location the simulated contours begin to deviate from their elliptical shape as higher order contributions to the mismatch become important. Fortunately, since by design, the mismatch is the loss in expected

SNR one would typically only ever place templates according to mismatches $\mathcal{O}(10\%)$ so as to recover a large enough fraction of the SNR to avoid missing any signals. We note that in this region the predicted mismatch using the metric approximation would have discrepancies relative to the true mismatch at a level $< 0.1\%$.

The re-parameterization of the phase into the \mathbf{u} coordinates is in fact entirely equivalent to the approximations made in so-called acceleration searches [1–3]. Here, in just the same way as in an acceleration search, the length of coherent observation coupled with the orbital period determines how many orders of expansion are required to accurately model the phase. Conversely, given a computationally limited number of expansion terms, there is a corresponding limit to the shortest orbital period that can be searched for a given coherent observation time. Based on worst case values of t_{asc} in relation to t_{mid} we find that

$$(\Omega\Delta T) \lesssim \left(\frac{\Delta\Phi(n+1)!}{2\pi a\nu} \right)^{1/(n+1)}, \quad (22)$$

represents a limit on the length of the coherent observations for an n 'th order expansion in the \mathbf{u} coordinates where $\Delta\Phi$ is the allowed error in phase between signal and model. For example, in order to model a $\nu = 100$ Hz signal with a projected semi-major axis $a = 1$ second with error in signal phase $\Delta\Phi = \pi/2$ using only an $n = 2$ expansion we would be limited to coherent observations spanning up to $\approx 1/25$ of an orbit.

The number of templates required to cover a parameter space is proportional to its proper volume, the integral of the square-root of the metric determinant over the parameter space, and is given by

$$\mathcal{N} = \xi(n, \mu) \int_{\mathcal{S}} d\theta \sqrt{\det g} \quad (23)$$

where we have used \mathcal{S} to represent the parameter space and the template density $\xi(n, \mu)$ is a function of the dimensionality of the space n , the desired mismatch μ and the choice of lattice covering. This gives us

$$\mathcal{N}_{\text{co}}^{(u)} \propto \xi(n, \mu) \Delta T^{n(n+1)/2} \int_{\mathcal{S}} d^n u \quad (24)$$

as the number of templates required for a single segment. Note that we do not give the explicit scaling associated with the parameter space boundaries (as done below in Eqs. 28,29). The integral over the parameter space volume is a complicated function of these boundaries and will behave differently depending upon the relative sizes of the uncertainties in the orbital parameters e.g. well known orbital period with poorly known time of ascension compared to poorly known period and well known time of ascension. One of the simpler cases one can consider is one in which the time of ascension is completely unknown. In this case the parameter space boundaries in the \mathbf{u} space form a hypercube with limits $\nu_{\text{min}} < u_1 < \nu_{\text{max}}$ and $-a_{\text{max}} \nu_{\text{max}} \Omega_{\text{max}}^k < u_k < a_{\text{max}} \nu_{\text{max}} \Omega_{\text{max}}^k$ for $k > 1$ and the number of templates is given by

$$\mathcal{N}_{\text{co}}^{(u)} \propto \xi(n, \mu) \Delta T^{n(n+1)/2} (\nu_{\text{max}} - \nu_{\text{min}}) (a_{\text{max}} \nu_{\text{max}})^{n-1} \Omega_{\text{max}}^{n(n+1)/2-1}. \quad (25)$$

the inclusion of the off-diagonal terms has insignificant effect. Significant correlations would reduce the volume element and ultimately lead to a reduction in the number of templates because individual templates would occupy more space. If we consider, for example, the parameters ν and a we find that by including the off-diagonal term in the calculation of the sub-volume element the fractional reduction in the volume is $\approx a^2 \Omega^2 / 4$ which is negligible for all practical orbital parameter values.

The reason that the metric becomes approximately diagonal and that therefore parameter correlations are removed can be explained as follows. The analysis of each segment can be viewed as an independent measurement of the signal and its parameters. Recall that we use templates placed in the \mathbf{u} space rather than the physical parameter space $\boldsymbol{\theta}$ because of degeneracies in the physical parameters for short observation times. This simply means that our ability to determine certain physical parameters and certain physical parameter combinations is poor in this choice of coordinates.

For example, imagine a segment coinciding with a small fraction of the orbit that places the source at the ascending node of the orbit. In this case the source is moving towards us at its greatest speed. We will also focus on a single parameter pair, the intrinsic frequency ν and the projected orbital semi-major axis a but note that the proceeding arguments apply equally well to all other parameters. At this segment epoch we are essentially measuring the maximally Doppler modulated signal frequency $\approx \nu(1 + a\Omega)$ Hz and we therefore find that there exists a degeneracy making us unable to disentangle the true value of the frequency from that of the projected semi-major axis. The signal can equally well be estimated within this segment as having a higher frequency and smaller semi-major axis or vice versa. In this sense we would say that there exists a negative correlation between these parameters. A negative (or positive) correlation implies that an increase in mismatch from a positive offset in one of the parameters can be counteracted by a negative (positive) offset in the other.

If we now examine the behavior of the ν, a correlations at an orbital epoch advanced in time by $P/4$ seconds we find that the source is now moving perpendicular to the observer's line of sight. In this case the frequency is approximately constant for the duration of the segment and there would be little information in the signal regarding its orbital acceleration. There now exists no correlation between ν and a and one is able to determine the frequency quite accurately at the expense of relatively poor determination of the projected semi-major axis. Advance again by $P/4$ and the source is now receding from the observer at its maximum speed. We now see exactly opposite behavior to that seen for the initial epoch in that there now exists an equal in magnitude positive correlation between ν and a . Finally, advancing again by $P/4$ we find that the correlations have vanished just as for the epoch one half orbit earlier.

Under our assumptions that the total observation spans many orbits and that the short observations themselves are uniformly distributed over this span we obtain measurements from all orbital phases. The combination of a pair of measurements that have approximately equal and opposite correlations

will therefore remove those correlations. With many segments randomly positioned in orbital phase each one can be approximated as having a corresponding segment on the opposite side of the orbit. As such, each opposing pair of segments removes the correlations in the final semi-coherent measurement.

Shown in Fig. 2 are the results of numerical simulations whereby the mismatch $\hat{\mu}(\boldsymbol{\theta}, \Delta\boldsymbol{\theta})$ has been computed over the 6-dimensional parameter space surrounding a simulated signal. Overlaid on the plots within this figure are the analytically derived mismatch ellipses corresponding to solving Eq. 19 for $\hat{\mu} = 0.1$ using Eq. 27 as the semi-coherent metric. The simulation comprised of $M = 500$ coherently analyses $\Delta T = 200$ second long segments randomly distributed across an full observation span $\tau = 10^8$ seconds. The simulated signal has an orbital angular frequency $\Omega = 10^{-4}$ rads s^{-1} (orbital period of 17.45 hours), a frequency $\nu = 200$ Hz, an orbital semi-major axis $a = 1$ second and an eccentricity $e = 0.02$ and argument of periapse $\omega = 1$. It is clear that in this case the approximations made in the Taylor expansion and discarding of the off-diagonal metric elements were valid since there is no indication of correlation between parameters. Correlations would appear as ellipsoidal mismatch contours with semi-minor and semi-major axes inclined with respect to the parameter axes, i.e. tilted ellipses as seen in some panels of Fig. 1. We also see again at large $\mu > 0.1$ mismatches, effects due to the breakdown of the quadratic approximation used in the definition of the metric. These deviations from ellipticity, seen the simulated mismatch contours, can also be attributed to the finite number ($M = 500$) of segments randomly distributed over the observation span. This is due to the fact that the mechanism through which one can assume the disappearance of the off-diagonal metric elements is applicable only in the limit where the number of segments $M \gg 1$. We note however, that in the region of interest around $\mu \sim 10\%$ the discrepancy between the metric approximation and our simulation is $< 1\%$. To place this in a practical context, using this metric to place templates with an expected maximum mismatch between signal and template of 10%, in a worst case scenario could result in a true mismatch of $\approx 11\%$.

Using the metric result we can compute the number of semi-coherent templates required for a search and the scalings associated with the parameter space dimensions. Considering the full $n = 6$ low-eccentricity orbit system we obtain

$$\begin{aligned} N_{\text{semi}} = & \frac{\pi^6}{16 \sqrt{6} \mu^3} \Delta T^6 \tau \left(\nu_{\text{max}}^6 - \nu_{\text{min}}^6 \right) \left(a_{\text{max}}^5 - a_{\text{min}}^5 \right) \\ & \times \left(\Omega_{\text{max}}^7 - \Omega_{\text{min}}^7 \right) (t_{\text{asc,max}} - t_{\text{asc,min}}) e_{\text{max}}, \quad (28) \end{aligned}$$

where we have defined the parameter space \mathcal{S} as a 6-dimensional cube bounded by the minimum and maximum ranges of the parameter vector $\boldsymbol{\theta}$. We have used the relation $dkd\eta = e |\cos(2\omega)| ded\omega$ in computing the integral over the eccentricity parameters. We have used lower and upper bounds of zero and e_{max} respectively for eccentricity and assumed that the argument of periapse would always be completely unknown and hence would have a range of zero to 2π . Note that for the template density we have assumed sub-optimal template placement based on a hyper-cubic lattice. A reduction

of a factor of ≈ 6.8 can be achieved if an A_n^* lattice is used in this $n = 6$ case.

We show in Fig. 3 the regions of parameter space for which a semi-coherent search would require coverage in the eccentricity parameters κ and η . This requirement is strongly dependent on the length of the constituent coherent observations, the product of the frequency and semi-major axis, and the eccentricity itself. As stated earlier, for the majority of our primary sources, the LMXBs, the expected eccentricities in these systems are relatively low (typically $< 10^{-3}$). In addition, the computational limitations imposed by the size of the remaining parameter space forces the coherent observation length to shorter times. This leads us to the conclusion that in general a circular orbit phase model will be applicable to the LMXB sources. For a circular orbit system, ignoring the κ and η dimensions, we have the following template scalings

$$\mathcal{N}_{\text{semi}}^{\text{circ}} = \frac{\pi^4}{36 \sqrt{6} \mu^2} \Delta T^4 \tau (v_{\text{max}}^4 - v_{\text{min}}^4) (a_{\text{max}}^3 - a_{\text{min}}^3) \times (\Omega_{\text{max}}^5 - \Omega_{\text{min}}^5) (t_{\text{asc,max}} - t_{\text{asc,min}}). \quad (29)$$

Note that again we have assumed a sub-optimal hyper-cubic template lattice and in this $n = 4$ case a factor of ≈ 2.8 reduction in templates can be achieved using an A_n^* lattice. We wish to stress that common mistakes made in estimating the required number of templates stem from the inclusion of dimensions that are geometrically “thinner” than the mismatch coverage of a single template. Such mistakes can lead to severe underestimation of the number of required templates. For example, take the parameters of the simulations for which results are shown in Fig. 2 and apply them to Fig. 3 which shows the requirements of a semi-coherent search with regards to placing templates in the eccentricity parameters. We see that for $\Omega \Delta T = 0.02$ and $va = 200$ the corresponding eccentricity threshold is ≈ 0.1 . We would therefore expect a semi-coherent search to be unable to distinguish eccentric orbits from circular orbits for eccentricities below this value. Looking at the mismatch ellipses shown in Fig. 2 we see that this is indeed the case, the scale of the ellipses in the κ and η dimensions

($\kappa^2 + \eta^2 = e^2$) is ~ 0.1 whereas the signal has eccentricity $e = 0.02$. This is a clear example of when one should assume a circular orbit model and remove the eccentricity and argument of periape from the analysis.

The linear dependence of the number of templates on the total observation span τ in both the eccentric and circular orbit cases indicates that an increase in observation span results in an increase in the number of templates. One can view this as a “refinement” of the semi-coherent template bank with increasing observation span. For our case this refinement comes from a single metric element, $G_{\Omega\Omega}$, and governs the template spacing in orbital angular frequency alone. The reason that we see this behavior is that the way in which we combine segments in this regime is a function of the orbital angular frequency (or equivalently the orbital period). In order to combine short coherent segments over increasingly large separations in time, one must have an increasingly accurate determination of the orbital phase. In short, the longer the observation span the more accurately one can determine the orbital period and hence more templates must be used to cover the corresponding search dimension Ω .

C. The coherent and semi-coherent metric for long ($\Delta T \gg P$) coherent segments

If the uncertainties in each of the parameter space dimensions is sufficiently small or the available computational power is large enough then one may be able to work in the regime $\Omega \Delta T \gg 1$. In this case one would be able to construct a search for which it is possible to achieve a coherent observation length greater than the length of the orbital period. The metric components can then be approximated by taking the limit in the regime $\Omega \Delta T \gg 1$ (given in Appendix C). Note that in this regime the physical coordinates $\theta = \{v, a, t_{\text{asc}}, \Omega, \kappa, \eta\}$ (as used for the semi-coherent metric) are a sensible choice upon which to base our metric. The metric on a coherent data segment can then be well approximated by

$$\lim_{\Delta T \gg P} g(\theta) \approx \begin{bmatrix} g_{vv} & & & & & & \\ & g_{aa} & & & & & \\ & & g_{t_{\text{asc}} t_{\text{asc}}} & & & & \\ & & & g_{\Omega\Omega} & & & \\ & & & & g_{\kappa\kappa} & & \\ & & & & & & g_{\eta\eta} \end{bmatrix} = \frac{1}{6} \pi^2 \begin{bmatrix} 2\Delta T^2 & & & & & & \\ & 12v^2 & & & & & \\ & & 12(va\Omega)^2 & & & & \\ & & & (va\Delta T)^2 & & & \\ & & & & 3(va)^2 & & \\ & & & & & & 3(va)^2 \end{bmatrix}. \quad (30)$$

where non-zero off-diagonal terms have been approximated as equal to zero. We justify this in the same way as done for our similar approximation to the semi-coherent metric in Eq. 27. Just as in the semi-coherent case, the off-diagonal terms constitute negligible correlations and their inclusion leaves the metric determinant essentially unchanged.

In Fig. 4 we see the degree of agreement between mismatches predicted by the approximate metric and those generated by signal injections (using Eq. 2 as the signal model). Again we see that our diagonal metric approximation is validated by the clear lack of correlation between parameters and that the discrepancy between approximated and simulated

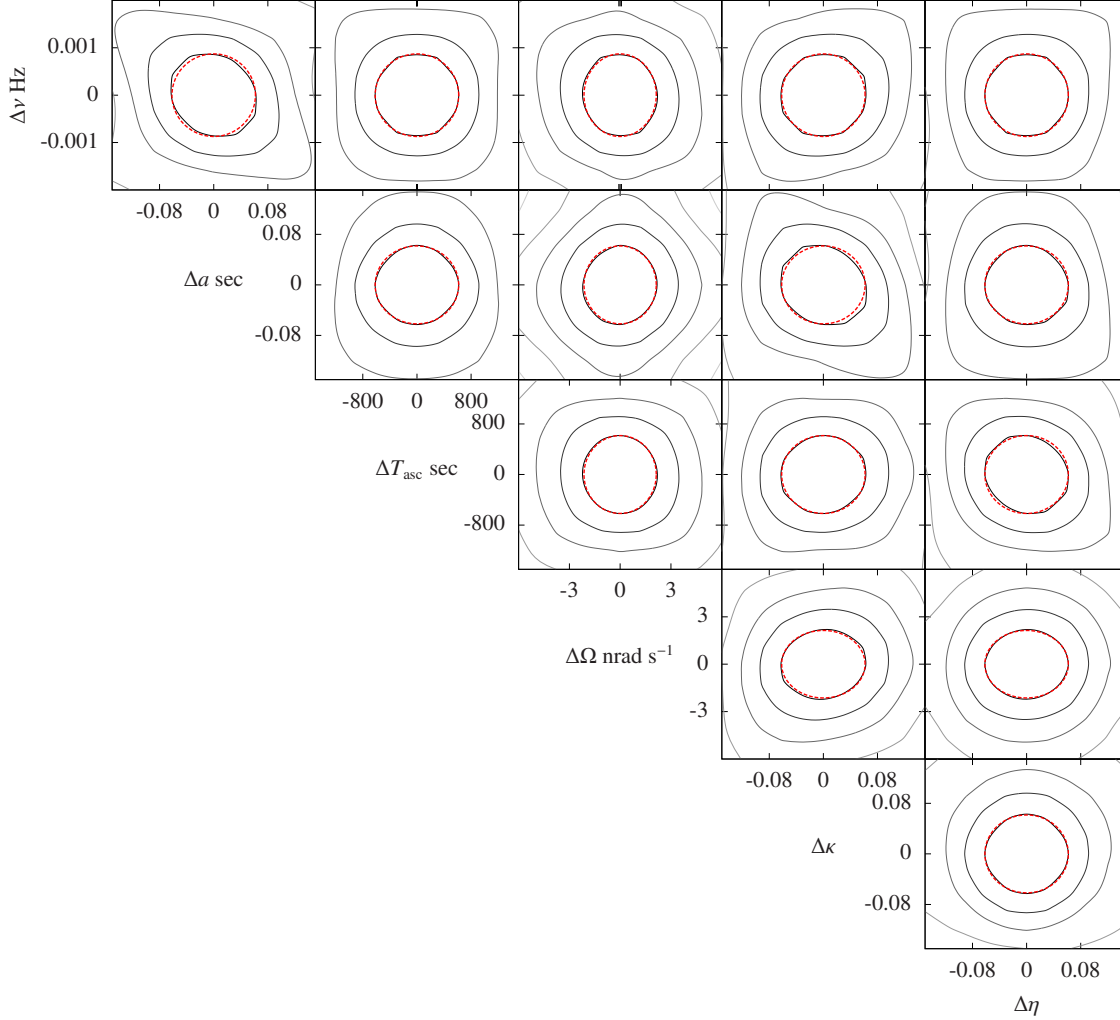


FIG. 2: The results of a simulation in which the mismatch $\mu(\theta, \Delta\theta)$ has been computed over a region in the 6-dimensional parameter space around the location of a simulated signal. The simulation modeled 500 individual coherently analyzed segments each of 200 seconds length spread over a period of $\tau = 10^8$ seconds. The signal parameters were $\nu = 200$, $a = 1$, $\Omega = 10^{-4}$ rads s $^{-1}$, $e = 0.02$ and $\omega = 1$ (t_{asc} chosen randomly from the range $[-P/2, P/2]$). Each panel shows the mismatch as a function of each pair of parameters where the mismatch has been maximized over all other parameters. The solid black and grey contours indicate the measured mismatch ranging from $\mu = 0.1$ (black) in steps of 0.1. The dashed red ellipses are those calculated using the approximate metric given in Eq. 27.

mismatches in this case is $<0.1\%$. Note that unlike the metric on the \mathbf{u} parameters this metric is independent of the epoch of each segment and hence a template bank generated from Eq. 30 can always be identical in equal length segments. This type of implementation, as we will see in the following section, can make the combination of results from many segments a far easier task than for a search using the \mathbf{u} coordinates. In addition, it makes the construction of the semi-coherent metric very simple. Since the semi-coherent metric is equal to the “average” metric (averaged over segments) and in this case the coherent metric remains unchanged for equal length seg-

ments, the semi-coherent metric is

$$\lim_{\Delta T \gg P} G(\theta) = \lim_{\Delta T \gg P} g(\theta) \quad (31)$$

and is therefore identical to the coherent metric given in Eq. 30.

We can again compute the scalings associated with the number of templates required to cover our 6-dimensional pa-

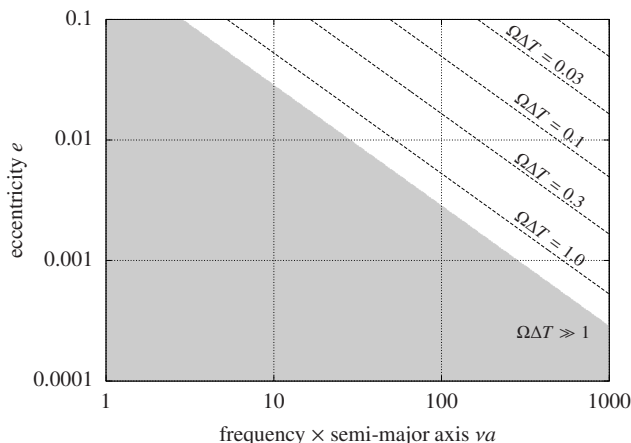


FIG. 3: An orbital parameter sub-space represented as the eccentricity versus the product of the signal frequency and projected semi-major axis. The dashed lines correspond to the semi-coherent metric’s requirement for templates in the eccentricity parameters κ and η . Each line represents a different coherent observation length measured in units of $\Omega\Delta T$. Above each dashed curve a semi-coherent analysis would require templates in the eccentricity parameters for a mismatch $\mu = 0.1$. Correspondingly, as the coherent integration time increases (relative to the orbital period) a limit is achieved at the boundary of the shaded region. Below this limit one need not include eccentricity in the signal model.

parameter space as done in Eqs. 28 and 24 giving us

$$\begin{aligned} \mathcal{N}_{\text{co}} = \mathcal{N}_{\text{semi}} = & \frac{9\sqrt{2}}{\pi^6\mu^3}\Delta T^2 (v_{\text{max}}^6 - v_{\text{min}}^6)(a_{\text{max}}^5 - a_{\text{min}}^5) \\ & \times (\Omega_{\text{max}}^2 - \Omega_{\text{min}}^2)(t_{\text{asc,max}} - t_{\text{asc,min}})e_{\text{max}}, \end{aligned} \quad (32)$$

where we note that as done in the previous template number estimates, we assume that each dimension has a thickness greater than the width of a single template span in the corresponding dimension. For the circular orbit case we obtain

$$\begin{aligned} \mathcal{N}_{\text{co}}^{\text{circ}} = \mathcal{N}_{\text{semi}}^{\text{circ}} = & \frac{\pi^4}{27\mu^2}\Delta T^2 (v_{\text{max}}^4 - v_{\text{min}}^4)(a_{\text{max}}^3 - a_{\text{min}}^3) \\ & \times (\Omega_{\text{max}}^2 - \Omega_{\text{min}}^2)(t_{\text{asc,max}} - t_{\text{asc,min}}). \end{aligned} \quad (33)$$

In both eccentric and circular orbit cases we have assumed a sub-optimal hyper-cubic lattice of templates. As stated in the previous section, reductions of factors of ≈ 6.8 and ≈ 2.8 can be achieved in the numbers of templates for the eccentric and circular orbit cases respectively if an A_n^* lattice is used.

We note that the number of templates in both the eccentric and circular orbit cases does not depend on the total observation span τ . This means that there is no “refinement” in the template bank as one uses larger numbers of segments. In contrast to the previously investigated regime $\Delta T \ll P$, if there is an offset in the orbital period then the mismatch from one segment will be identical to the mismatch from all other segments which will consequently be identical to the total mismatch. In

short, this is because there are no parameters in our model for which fractional losses in SNR accumulate beyond a single orbital period e.g. if there are offsets in all parameters, the fractional SNR loss after one orbit will be identical to the total fractional SNR loss after the next. This is in contrast to the behavior of the metric and mismatch in the $\Delta T \ll P$ regime discussed in Section II A. However, for the same volume of parameter space, a significantly larger number of templates would be required in the coherent stage for segment lengths that far exceed the orbital period compared to the case when the orbital period far exceeds the segment length.

III. DISCUSSION

We have presented a brief review of the phase model for continuously emitting sources in binary systems together with a review of the parameter space metric defined on the fractional loss in SNR when offset from the true signal location in parameter space. We then proceeded to apply the latter to the former to construct the semi-coherent parameter space metric for application to searches for such systems in noisy data. In addition we provide the outline for the practical application of a search strategy employing the semi-coherent metric in the opposing limits that the segments that are analyzed coherently span small fractions of the source orbital period and have durations far greater than the orbital period.

We have shown that in the short duration segment regime the semi-coherent metric on the physical parameters θ becomes approximately diagonal and hence the correlations between parameters are removed. This we attribute to the averaging procedure applied to the metric elements and the specific behavior of these elements as a function of orbital phase corresponding to each segment epoch. Whilst the metric itself is still a function of location within the parameter space making lattice based template placement difficult, the lack of parameter correlations does somewhat simplify the procedure. We note that for the short duration coherent segment scenario there is only one term in the semi-coherent metric that depends on the semi-coherent observation span. This is the element that determines the precision with which the orbital angular frequency must be sampled (and conversely the precision with which it can be determined in the limit of low signal-to-noise ratio). For all other parameters the equivalent precisions depend only upon the coherent observation time, the signal frequency, orbital angular frequency and semi-major axis. This result is identical in nature to that obtained in [19] where it was found that only one parameter in their isolated pulsar model, the pulsar spin derivative, was responsible for refinement of the template bank. The explanation is similar for both cases, both the spin derivative and orbital period, in each search respectively, determine how results from individual segments are combined whereas the other parameters do not. It is only the parameter Ω that is capable of causing an ever increasing offset in the orbital phase (just as the spin derivative in [19] is capable of causing a similarly increasing offset in signal phase). As such, coherent templates within increasingly separated segments would ex-

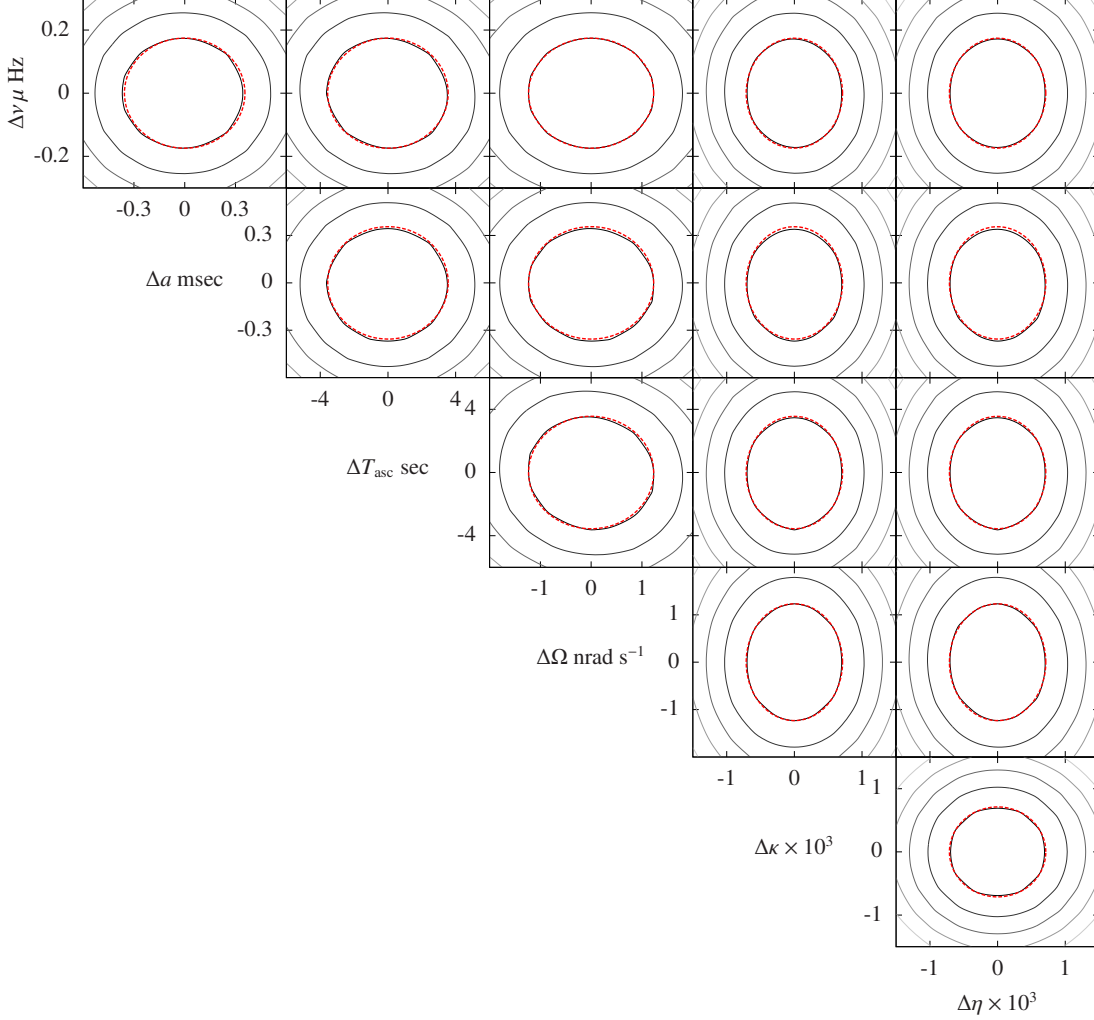


FIG. 4: The results of a simulation in which the mismatch $\mu(\lambda)$ has been computed over a region in the 6-dimensional parameter around the location of a simulated signal. The simulation modeled a single coherently analyzed segment of 10^6 seconds length containing a signal with parameters $\nu = 200$ Hz, $a = 1$ sea, $\Omega = 10^{-4}$ rads sec⁻¹, sea, $e = 0.005$ and $\omega = 1$ rad (t_{asc} chosen randomly from the range $[-P/2, P/2]$). Each panel shows the mismatch as a function of each pair of parameters where the mismatch has been maximized over all other parameters (these are not slices). The solid black and grey contours indicate the measured mismatch ranging from $\mu = 0.1$ (black) in steps of 0.1. The dashed red ellipses are those calculated using the approximate metric given in Eq. 30.

perience increasing mismatch for a constant offset in Ω . In contrast, an offset in the time of orbital ascension (assuming an exactly known orbital period) would cause the orbital phase to be offset by a constant amount in all segments. Consequently the mismatch would also be constant and hence the average mismatch, equivalent to the total semi-coherent mismatch, would also be constant with respect to the observation span τ . The consequence of this refinement on the orbital angular frequency parameter is that the cost of the semi-coherent stage of the analysis can dominate the cost of the coherent stage. However, one is always able to tune the relative costs by choosing a shorter or longer segment length. We leave the analysis of how to optimally make such choices for future

work.

When the duration of the coherent segments are much greater than the orbital period there is no dependence upon the total observation span and the semi-coherent metric is simply equal to the coherent metric since it is constant for each segment. In addition, just as for the short segment regime we find that the metric is diagonal and that there are therefore no parameter correlations. The independence of the total observation span on the metric can be explained by the fact that there is no dependence upon any of the parameters in the process of combining the results from each segment. In contrast to the short segment regime, one need not know the orbital angular frequency to map a set of physical parameters in one segment

to the corresponding (identical) set in another segment. This does not mean that parameter estimation is not enhanced with the addition of more segments over a longer observation span. In this case it is the semi-coherent accumulation of SNR that improves parameter estimation whilst the template density remains constant.

One interesting point to make given this result is the comparison between the different template scalings with the observation parameters for the short and long coherent duration regimes. For a fixed set of boundaries in the full 6-dimensional parameter space there appears to exist an observation span at which it becomes favorable (in terms of using fewer semi-coherent templates) to expand the coherent observation time to be consistent with the long coherent regime. This is because the template scaling with ΔT is steeper for the short segment compared to the long segment scenario. The point at which this occurs is dependent upon many interdependent factors including the volume of the parameter space, the relative uncertainties in each dimension and how many orders are included in the Taylor expansion in the \mathbf{u} coordinates. This statement is also under the assumption that the majority of the computational cost goes into computing the semi-coherent detection statistic and that the cost of computation of the individual segment statistics is negligible and that the computational cost of a long duration template is equal to that of a short duration template. It also neglects the issue that for a short coherent duration some dimensions are likely to not require templates. This occurs when the template span is greater than the parameter space range in that dimension. Note for example the metric elements corresponding to the eccentricity parameters κ and η for the short and long segment regimes. The template spacing in a given dimension is proportional to the inverse of the square-root of the corresponding metric element. The ratio between the short and long segment κ template spacing is $\sqrt{3}/(\Omega\Delta T_s)$ where ΔT_s here is the short segment duration. Dependent upon the uncertainty in κ , this may mean that templates are simply not required in the κ dimension for the short segment but are required in the long segment regime. If we look at all the contrasting template sizes in the short and long duration coherent segments regimes we see that in all dimensions except the spin frequency ν and the orbital angular frequency Ω , a template span is greater by a factor $\propto 1/(\Omega\Delta T) \gg 1$. The same factor for the spin frequency metric components is simply equal to the ratio of the short and long observation lengths $\Delta T_s/\Delta T_l$ and for templates in the orbital angular frequency dimension the same ratio is given by $\Omega\tau(\Delta T_s/\Delta T_l)$. This final result gives the false impression that by using short coherent segments one is able to better determine the orbital angular frequency of a source than by using long segments. We stress here that template placement is related to, but not equivalent to, parameter estimation. Template

placement using the metric defined on fractional SNR (\propto the log-likelihood) loss determines how finely a parameter space must be sampled in order to avoid missing a potential signal. Parameter estimation makes use of the likelihood itself and it's accuracy improves with SNR.

We mention at this point that the reader may question our choice of phase model parameterization. It is true that parameterizations like $x = a \cos(\Omega t_{asc}), y = a \sin(\Omega t_{asc})$ would potentially simplify the metric calculations and that a rescaling of the frequency parameter could do the same. However, since a general ‘‘fix-all’’ re-parameterization eludes the author, it was decided that the physical parameters were justifiable choices. The fact that the metric elements are functions of the parameters themselves is problematic from an implementation sense since this will potentially make template placement more complicated. Conversely, the parameter choice leads to a clearer understanding of how the semi-coherent metric scales with the unambiguous physical parameters of the system.

In conclusion, in deriving the semi-coherent metric for known binary systems we have provided a necessary tool for the continued sensitivity improvement of searches for continuously emitting sources of EM and GW emission. With focus on GW searches the advanced detector [34] era is fast approaching and LMXBs are an ever more realistic detection target. The optimality of search sensitivity at fixed computational cost has been approximately achieved by the Einstein@Home GW searches [35] for unknown isolated neutron stars (NSs). The achievement has arisen through the application of semi-coherent search strategies described in [19] and are similar to those outlined in this work. It is our hope that search strategies based on the semi-coherent methods described here will be employed in searches for the prime GW LMXB targets such as Sco X-1 and Cyg X-2.

Acknowledgments

We would like to thank Karl Wette, Evan Goetz, Holger Pletsch, Reinhard Prix, and the LIGO Scientific Collaboration continuous waves working group for many useful discussions.

Appendix A: Re-parameterized phase coordinates

In Section II A there is reference to a re-parameterization of the phase approximation given by Eq. 4 into the \mathbf{u} coordinates used in Eq. 20. The $\mathbf{u}^{(m)}$ coordinates for the m 'th segment are mapped onto the physical parameters θ via

$$\Phi_0^{(m)} = \frac{\Phi_0}{2\pi} + \nu(t + t_{\text{mid}}^{(n)} - t_{\text{ref}}) - av \left(\frac{\eta}{2} (3 + \cos[2(t - t_{\text{asc}} + t_{\text{mid}}^{(n)})\Omega]) - \sin[(t - t_{\text{asc}} + t_{\text{mid}}^{(n)})\Omega] - \frac{\kappa}{2} \sin[2(t - t_{\text{asc}} + t_{\text{mid}}^{(n)})\Omega] \right), \quad (\text{A1})$$

$$u_1^{(m)} = \nu + av\Omega(\cos[(t - t_{\text{asc}} + t_{\text{mid}}^{(n)})\Omega] + \kappa \cos[2(t - t_{\text{asc}} + t_{\text{mid}}^{(n)})\Omega] + \eta \sin[2(t - t_{\text{asc}} + t_{\text{mid}}^{(n)})\Omega]), \quad (\text{A2})$$

$$u_2^{(m)} = av\Omega^2 \left(2\eta \cos[2(t - t_{\text{asc}} + t_{\text{mid}}^{(n)})\Omega] - \sin[(t - t_{\text{asc}} + t_{\text{mid}}^{(n)})\Omega] - 2\kappa \sin[2(t - t_{\text{asc}} + t_{\text{mid}}^{(n)})\Omega] \right), \quad (\text{A3})$$

$$u_3^{(m)} = -av\Omega^3 \left(\cos[(t - t_{\text{asc}} + t_{\text{mid}}^{(n)})\Omega] + 4\kappa \cos[2(t - t_{\text{asc}} + t_{\text{mid}}^{(n)})\Omega] + 4\eta \sin[2(t - t_{\text{asc}} + t_{\text{mid}}^{(n)})\Omega] \right), \quad (\text{A4})$$

$$u_4^{(m)} = -av\Omega^4 \left(8\eta \cos[2(t - t_{\text{asc}} + t_{\text{mid}}^{(n)})\Omega] - \sin[(t - t_{\text{asc}} + t_{\text{mid}}^{(n)})\Omega] - 8\kappa \sin[2(t - t_{\text{asc}} + t_{\text{mid}}^{(n)})\Omega] \right). \quad (\text{A5})$$

Note that we give expressions only up to 4th order in time. If higher orders are required then it is likely that the coherent observation time spans a large fraction (or more) of a single orbital period. In this regime using the Taylor-expanded phase may not be a sensible choice and it may be more practical to use the fully coherent metric on the physical parameters.

$\{\nu, a, t_{\text{asc}}, \Omega, \kappa, \eta\}$ in the limit $\Delta T \gg P$ and $\Omega\Delta T \gg 1$ are

Appendix B: Coherent metric elements for long ($\Delta T \gg P$) segment lengths

To leading order in κ and η (where appropriate) the elements of the coherent metric on the physical parameters space $\theta =$

$$g_{\nu\nu} = \frac{\pi^2 \Delta T^2}{3} \quad (\text{B1})$$

$$g_{aa} = 2\pi^2 v^2 \left(1 + \frac{e^2}{4}\right) \quad (\text{B2})$$

$$g_{t_{\text{asc}} t_{\text{asc}}} = 2\pi^2 v^2 a^2 \Omega^2 (1 + e^2) \quad (\text{B3})$$

$$g_{\Omega\Omega} = \frac{1}{6} \pi^2 v^2 a^2 \Delta T^2 (1 + e^2) \quad (\text{B4})$$

$$g_{\kappa\kappa} = \frac{1}{2} a^2 \pi^2 v^2 \quad (\text{B5})$$

$$g_{\eta\eta} = \frac{1}{2} a^2 \pi^2 v^2 \quad (\text{B6})$$

$$g_{\nu a} = g_{a\nu} = 2\pi^2 v \left\{ a \left(1 + \frac{e^2}{4}\right) - \frac{2}{\Omega} \cos\left(\frac{\Delta T \Omega}{2}\right) \cos(\Omega t_{\text{asc}}) + \frac{1}{\Omega} \cos(\Omega \Delta T) [\eta \sin(2\Omega t_{\text{asc}}) - \kappa \cos(2\Omega t_{\text{asc}})] \right\} \quad (\text{B7})$$

$$g_{\nu t_{\text{asc}}} = g_{t_{\text{asc}} \nu} = 4a\pi^2 v \left\{ \cos\left(\frac{\Delta T \Omega}{2}\right) \sin(\Omega t_{\text{asc}}) + \frac{1}{2} \cos(\Delta T \Omega) [\eta \cos[2\Omega t_{\text{asc}}] + \kappa \sin(2\Omega t_{\text{asc}})] \right\} \quad (\text{B8})$$

$$g_{\nu\Omega} = g_{\Omega\nu} = \frac{2\pi^2 v a \Delta T}{\Omega} \left\{ \cos(\Omega t_{\text{asc}}) \sin\left(\frac{\Delta T \Omega}{2}\right) + \frac{1}{2} \sin(\Omega \Delta T) [\kappa \cos(2\Omega t_{\text{asc}}) - \eta \sin(2\Omega t_{\text{asc}})] \right\} \quad (\text{B9})$$

$$g_{\nu\kappa} = g_{\kappa\nu} = -\frac{\pi^2 v a}{\Omega} \cos(\Omega \Delta T) \cos(2\Omega t_{\text{asc}}) + \frac{1}{2} \pi^2 v a^2 \kappa \quad (\text{B10})$$

$$g_{\nu\eta} = g_{\eta\nu} = \frac{\pi^2 v a}{\Omega} \cos(\Omega \Delta T) \sin(2\Omega t_{\text{asc}}) + \frac{1}{2} \pi^2 v a^2 \eta \quad (\text{B11})$$

$$g_{a t_{\text{asc}}} = g_{t_{\text{asc}} a} = 0 \quad (\text{B12})$$

$$g_{a\Omega} = g_{\Omega a} = -\frac{\pi^2 v^2 a}{\Omega} \left\{ \cos(\Omega \Delta T) \cos(2\Omega t_{\text{asc}}) + \kappa \cos\left(\frac{\Omega \Delta T}{2}\right) \left[\cos(\Omega t_{\text{asc}}) + \cos(3\Omega t_{\text{asc}}) [1 - 2 \cos(\Omega \Delta T)] \right] \right. \\ \left. + 2\eta \cos\left(\frac{\Omega \Delta T}{2}\right) \sin(\Omega t_{\text{asc}}) \left[\cos(\Omega \Delta T) [1 + 2 \cos(2\Omega t_{\text{asc}})] - \cos(2\Omega t_{\text{asc}}) - 1 \right] \right\} \quad (\text{B13})$$

$$g_{a\kappa} = g_{\kappa a} = \frac{1}{2} \pi^2 v^2 a \kappa \quad (\text{B14})$$

$$g_{a\eta} = g_{\eta a} = \frac{1}{2} \pi^2 v^2 a \eta \quad (\text{B15})$$

$$g_{t_{\text{asc}} \Omega} = g_{\Omega t_{\text{asc}}} = \pi^2 v^2 a^2 \left\{ \cos(\Omega \Delta T) \sin(2\Omega t_{\text{asc}}) + 2\Omega t_{\text{asc}} \right. \\ \left. + \frac{4\eta}{3} \cos\left(\frac{\Omega \Delta T}{2}\right) [3 \cos(\Omega t_{\text{asc}}) + \cos(3\Omega t_{\text{asc}}) (2 \cos(\Omega \Delta T) - 1)] \right. \\ \left. + \frac{4\kappa}{3} \cos\left(\frac{\Omega \Delta T}{2}\right) [3 \sin(\Omega t_{\text{asc}}) + \sin(3\Omega t_{\text{asc}}) (2 \cos(\Omega \Delta T) - 1)] \right\} \quad (\text{B16})$$

$$g_{t_{\text{asc}} \kappa} = g_{\kappa t_{\text{asc}}} = -\pi^2 v^2 a^2 \Omega \eta \quad (\text{B17})$$

$$g_{t_{\text{asc}} \eta} = g_{\eta t_{\text{asc}}} = \pi^2 v^2 a^2 \Omega \kappa \quad (\text{B18})$$

$$g_{\Omega\kappa} = g_{\kappa\Omega} = -\frac{\pi^2 v^2 a^2}{\Omega} \left\{ \frac{1}{3} \cos\left(\frac{\Omega \Delta T}{2}\right) [3 \cos(\Omega t_{\text{asc}}) + \cos(3\Omega t_{\text{asc}}) (2 \cos(\Omega \Delta T) - 1)] \right. \\ \left. + \frac{\eta}{4} [4\Omega t_{\text{asc}} - \cos(2\Omega \Delta T) \sin(4\Omega t_{\text{asc}})] + \frac{\kappa}{4} \cos(2\Omega \Delta T) \cos(4\Omega t_{\text{asc}}) \right\} \quad (\text{B19})$$

$$g_{\Omega\eta} = g_{\eta\Omega} = \frac{\pi^2 v^2 a^2}{\Omega} \left\{ \frac{1}{3} \cos\left(\frac{\Omega \Delta T}{2}\right) [3 \sin(\Omega t_{\text{asc}}) + \sin(3\Omega t_{\text{asc}}) (2 \cos(\Omega \Delta T) - 1)] \right. \\ \left. + \frac{\kappa}{4} [4\Omega t_{\text{asc}} + \cos(2\Omega \Delta T) \sin(4\Omega t_{\text{asc}})] + \frac{\eta}{4} \cos(2\Omega \Delta T) \cos(4\Omega t_{\text{asc}}) \right\} \quad (\text{B20})$$

$$g_{\kappa\eta} = g_{\eta\kappa} = 0 \quad (\text{B21})$$

Appendix C: Semi-coherent metric elements

Here we give the expressions for the metric elements in the eccentric orbit case for a phase model defined by Eq. 4 on

the set of parameters $\theta = \{\nu, a, t_{\text{asc}}, \Omega, \kappa, \eta\}$. The following elements are valid in the limits of $e \ll 1$ and for $\tau \gg \Delta T$ and $\tau \gg P$,

$$G_{\nu\nu} = \frac{\pi^2 \Delta T^2}{3} - \frac{\pi^2 a^2}{12 \Omega^2 \Delta T^2} (48 + 3e^2 - 24 \Delta T^2 \Omega^2 - 6e^2 \Delta T^2 \Omega^2 - 48 \cos(\Delta T \Omega) - 3e^2 \cos(2 \Delta T \Omega)) \quad (\text{C1})$$

$$G_{aa} = 2\pi^2 \nu^2 \left\{ 1 + \frac{e^2}{4} - \frac{2}{\Omega^2 \Delta T^2} \left[1 - \cos(\Omega \Delta T) + \frac{e^2}{16} - \frac{e^2}{16} \cos(2\Omega \Delta T) \right] \right\} \quad (\text{C2})$$

$$G_{t_{\text{asc}} t_{\text{asc}}} = 2\pi^2 \nu^2 a^2 \Omega^2 \left\{ 1 + e^2 - \frac{2}{\Omega^2 \Delta T^2} \left[1 - \cos(\Omega \Delta T) + \frac{e^2}{4} - \frac{e^2}{4} \cos(2\Omega \Delta T) \right] \right\} \quad (\text{C3})$$

$$G_{\Omega\Omega} = \frac{1}{6} a^2 \pi^2 \nu^2 \Delta T^2 \left\{ 1 + e^2 - \frac{1}{2\Omega^2 \Delta T^2} [4 - 4 \cos(\Omega \Delta T) + e^2 - e^2 \cos(2\Omega \Delta T)] \right\} \quad (\text{C4})$$

$$G_{\kappa\kappa} = 2a^2 \nu^2 \pi^2 \left[1 - \frac{(1 - \cos(2\Omega \Delta T))}{8\Omega^2 \Delta T^2} \right] \quad (\text{C5})$$

$$G_{\eta\eta} = 2a^2 \nu^2 \pi^2 \left[1 - \frac{(1 - \cos(2\Omega \Delta T))}{8\Omega^2 \Delta T^2} \right] \quad (\text{C6})$$

$$G_{\nu a} = G_{a\nu} = 2\pi^2 \nu \left\{ 1 + \frac{e^2}{4} - \frac{2}{\Omega^2 \Delta T^2} \left[1 - \cos(\Omega \Delta T) + \frac{e^2}{16} - \frac{e^2}{16} \cos(2\Omega \Delta T) \right] \right\} \quad (\text{C7})$$

$$G_{\nu t_{\text{asc}}} = G_{t_{\text{asc}} \nu} = 0 \quad (\text{C8})$$

$$G_{\nu\Omega} = G_{\Omega\nu} = \frac{4\pi^2 \nu a^2}{\Omega^2 \Delta T^2} \left\{ 1 - \cos(\Omega \Delta T) + \frac{e^2}{16} - \frac{e^2}{16} \cos(2\Omega \Delta T) - \frac{e^2 \Omega \Delta T}{16} \sin(2\Omega \Delta T) \right\} \quad (\text{C9})$$

$$G_{\nu\kappa} = G_{\kappa\nu} = \frac{1}{2} \pi^2 \nu a^2 \kappa \left\{ 1 - \frac{1}{2\Omega^2 \Delta T^2} [1 - \cos(\Omega \Delta T)] \right\} \quad (\text{C10})$$

$$G_{\nu\eta} = G_{\eta\nu} = \frac{1}{2} \pi^2 \nu a^2 \eta \left\{ 1 - \frac{1}{2\Omega^2 \Delta T^2} [1 - \cos(\Omega \Delta T)] \right\} \quad (\text{C11})$$

$$G_{a t_{\text{asc}}} = G_{t_{\text{asc}} a} = 0 \quad (\text{C12})$$

$$G_{a\Omega} = G_{\Omega a} = \frac{4\pi^2 a \nu^2}{\Omega^2 \Delta T^2} \left\{ 1 - \cos(\Omega \Delta T) - \frac{\Omega \Delta T}{2} \sin(\Omega \Delta T) + \frac{e^2}{16} + \frac{e^2}{16} \cos(2\Omega \Delta T) - \frac{e^2 \Omega \Delta T}{16} \sin(2\Omega \Delta T) \right\} \quad (\text{C13})$$

$$G_{a\kappa} = G_{\kappa a} = \frac{1}{2} \pi^2 \nu^2 a \kappa \left\{ 1 - \frac{1}{2\Omega^2 \Delta T^2} [1 - \cos(2\Omega \Delta T)] \right\} \quad (\text{C14})$$

$$G_{a\eta} = G_{\eta a} = \frac{1}{2} \pi^2 \nu^2 a \eta \left\{ 1 - \frac{1}{2\Omega^2 \Delta T^2} [1 - \cos(2\Omega \Delta T)] \right\} \quad (\text{C15})$$

$$G_{t_{\text{asc}} \Omega} = G_{\Omega t_{\text{asc}}} = 2a^2 \pi^2 \nu^2 t_{\text{asc}} \left\{ 1 + e^2 - \frac{2}{\Omega^2 \Delta T^2} \left[1 + \frac{e^2}{4} - \cos(\Omega \Delta T) - \frac{e^2}{4} \cos(2\Omega \Delta T) \right] \right\} \quad (\text{C16})$$

$$G_{t_{\text{asc}} \kappa} = G_{\kappa t_{\text{asc}}} = -\pi^2 \nu^2 a^2 \eta \left\{ 1 - \frac{1}{2\Omega^2 \Delta T^2} [1 - \cos(2\Omega \Delta T)] \right\} \quad (\text{C17})$$

$$G_{t_{\text{asc}} \eta} = G_{\eta t_{\text{asc}}} = \pi^2 \nu^2 a^2 \kappa \left\{ 1 - \frac{1}{2\Omega^2 \Delta T^2} [1 - \cos(2\Omega \Delta T)] \right\} \quad (\text{C18})$$

$$G_{\Omega\kappa} = G_{\kappa\Omega} = -\frac{a^2 \nu^2 \pi^2}{4\Omega^3 \Delta T^2} (-\kappa - 2\eta t_{\text{asc}} \Omega + 4\eta \Delta T^2 t_{\text{asc}} \Omega^3 + (\kappa + 2\eta t_{\text{asc}} \Omega) \cos(2\Delta T \Omega) + \kappa \Delta T \Omega \sin(2\Delta T \Omega)) \quad (\text{C19})$$

$$G_{\Omega\eta} = G_{\eta\Omega} = \frac{a^2 \nu^2 \pi^2}{4\Omega^3 \Delta T^2} (\eta - 2\kappa t_{\text{asc}} \Omega + 4\kappa \Delta T^2 t_{\text{asc}} \Omega^3 - (\eta - 2\kappa t_{\text{asc}} \Omega) \cos(2\Delta T \Omega) - \eta \Delta T \Omega \sin(2\Delta T \Omega)) \quad (\text{C20})$$

$$G_{\kappa\eta} = G_{\eta\kappa} = 0. \quad (\text{C21})$$

The following metric elements are the Taylor-expanded versions, to leading order in $\Omega\Delta T$ and in ϵ , of those given above

$$G_{vv}^T = \frac{\pi^2 \Delta T^2}{3} \quad (C22)$$

$$G_{aa}^T = \frac{1}{6} \pi^2 v^2 \Omega^2 \Delta T^2 \quad (C23)$$

$$G_{t_{\text{asc}} t_{\text{asc}}}^T = \frac{1}{6} \pi^2 v^2 a^2 \Omega^2 \Delta T^2 \quad (C24)$$

$$G_{\Omega\Omega}^T = \frac{1}{72} \pi^2 v^2 a^2 \Omega^2 \Delta T^2 \tau^2 \quad (C25)$$

$$G_{\kappa\kappa}^T = \frac{1}{6} a^2 v^2 \pi^2 \Omega^2 \Delta T^2 \quad (C26)$$

$$G_{\eta\eta}^T = \frac{1}{6} a^2 v^2 \pi^2 \Omega^2 \Delta T^2 \quad (C27)$$

$$G_{va}^T = G_{av}^T = \frac{1}{6} \pi^2 av \Omega^2 \Delta T^2 \quad (C28)$$

$$G_{vt_{\text{asc}}}^T = G_{t_{\text{asc}}v}^T = 0 \quad (C29)$$

$$G_{v\Omega}^T = G_{\Omega v}^T = \frac{1}{6} \pi^2 a^2 v \Omega \Delta T^2 \quad (C30)$$

$$G_{v\kappa}^T = G_{\kappa v}^T = \frac{1}{6} \pi^2 a^2 v \kappa \Omega^2 \Delta T^2 \quad (C31)$$

$$G_{v\eta}^T = G_{\eta v}^T = \frac{1}{6} \pi^2 a^2 v \eta \Omega^2 \Delta T^2 \quad (C32)$$

$$G_{at_{\text{asc}}}^T = G_{t_{\text{asc}}a}^T = 0 \quad (C33)$$

$$G_{a\Omega}^T = G_{\Omega a}^T = \frac{1}{6} \pi^2 v^2 a \Omega \Delta T^2 \quad (C34)$$

$$G_{a\kappa}^T = G_{\kappa a}^T = \frac{1}{6} \pi^2 v^2 a \kappa \Omega^2 \Delta T^2 \quad (C35)$$

$$G_{a\eta}^T = G_{\eta a}^T = \frac{1}{6} \pi^2 v^2 a \eta \Omega^2 \Delta T^2 \quad (C36)$$

$$G_{t_{\text{asc}}\Omega}^T = G_{\Omega t_{\text{asc}}}^T = \frac{1}{6} \pi^2 v^2 a^2 t_{\text{asc}} \Omega^3 \Delta T^2 \quad (C37)$$

$$G_{t_{\text{asc}}\kappa}^T = G_{\kappa t_{\text{asc}}}^T = -\frac{1}{3} \pi^2 v^2 a^2 \eta \Omega^3 \Delta T^2 \quad (C38)$$

$$G_{t_{\text{asc}}\eta}^T = G_{\eta t_{\text{asc}}}^T = \frac{1}{3} \pi^2 v^2 a^2 \kappa \Omega^3 \Delta T^2 \quad (C39)$$

$$G_{\Omega\kappa}^T = G_{\kappa\Omega}^T = \frac{1}{6} \pi^2 v^2 a^2 \Delta T^2 (\kappa \Omega - 2\eta t_{\text{asc}} \Omega^2) \quad (C40)$$

$$G_{\Omega\eta}^T = G_{\eta\Omega}^T = \frac{1}{6} (a^2 \eta v^2 \pi^2 \Omega + 2a^2 \kappa v^2 \pi^2 t_{\text{asc}} \Omega^2) \Delta T^2 \quad (C41)$$

$$G_{\kappa\eta}^T = G_{\eta\kappa}^T = 0. \quad (C42)$$

The metric given in Eq. 27 is a further approximation in which the off-diagonal terms have been set to zero. This approximation is valid due to the fact that these terms cause only minor mismatch ellipse rotations in the physical parameter space. It

follows that the diagonal elements themselves are a very good approximation to the eigenvalues of the metric and the eigenvectors are very well aligned with the physical dimensions of the parameter space.

[1] S. B. Anderson, P. W. Gorham, S. R. Kulkarni, T. A. Prince, and A. Wolszczan, *nat* **346**, 42 (1990).

[2] S. R. Anderson, Ph.D. thesis, Illinois Inst. of Tech., Chicago. (1992).

[3] A. J. Faulkner, I. H. Stairs, M. Kramer, A. G. Lyne, G. Hobbs, A. Possenti, D. R. Lorimer, R. N. Manchester, M. A. McLaughlin, N. D'Amico, et al., *mnr*s **355**, 147 (2004), arXiv:astro-ph/0408228.

- [4] S. M. Ransom, J. M. Cordes, and S. S. Eikenberry, *apj* **589**, 911 (2003), arXiv:astro-ph/0210010.
- [5] J. W. T. Hessels, S. M. Ransom, I. H. Stairs, V. M. Kaspi, and P. C. C. Freire, *apj* **670**, 363 (2007), 0707.1602.
- [6] S. Ransom, J. Hessels, I. Stairs, V. Kaspi, P. Freire, and D. Backer, in *Binary Radio Pulsars*, edited by F. A. Rasio & I. H. Stairs (2005), vol. 328 of *Astronomical Society of the Pacific Conference Series*, pp. 199–+.
- [7] C. Messenger and G. Woan, *Classical and Quantum Gravity* **24**, 469 (2007), arXiv:gr-qc/0703155.
- [8] K. S. Wood, J. P. Norris, P. Hertz, B. A. Vaughan, P. F. Michelson, K. Mitsuda, W. H. G. Lewin, J. van Paradijs, W. Penninx, and M. van der Klis, *apj* **379**, 295 (1991).
- [9] B. A. Vaughan, M. van der Klis, K. S. Wood, J. P. Norris, P. Hertz, P. F. Michelson, J. van Paradijs, W. H. G. Lewin, K. Mitsuda, and W. Penninx, *ApJ* **435**, 362 (1994).
- [10] L. S. C. B. A. et al., *prd* **76**, 082001 (2007), arXiv:gr-qc/0605028.
- [11] L. S. C. B. A. et al., *prd* **76**, 082003 (2007), arXiv:astro-ph/0703234.
- [12] S. V. Dhurandhar and A. Vecchio, *prd* **63**, 122001 (2001), arXiv:gr-qc/0011085.
- [13] A. L. Watts, B. Krishnan, L. Bildsten, and B. F. Schutz, *mnras* **389**, 839 (2008), 0803.4097.
- [14] R. Balasubramanian, B. S. Sathyaprakash, and S. V. Dhurandhar, *Phys. Rev. D* **53**, 3033 (1996).
- [15] B. J. Owen, *Phys. Rev. D* **53**, 6749 (1996).
- [16] B. J. Owen and B. S. Sathyaprakash, *Phys. Rev. D* **60**, 022002 (1999).
- [17] P. R. Brady and T. Creighton, *Phys. Rev. D* **61**, 082001 (2000), arXiv:gr-qc/9812014.
- [18] H. J. Pletsch, *Phys. Rev. D* **78**, 102005 (2008), 0807.1324.
- [19] H. J. Pletsch and B. Allen, *Physical Review Letters* **103**, 181102 (2009), 0906.0023.
- [20] R. Blandford and S. A. Teukolsky, *Astrophys. J.* **205**, 580 (1976).
- [21] A. E. Roy, *Orbital motion* (Institute of Physics, 2005, 1988).
- [22] C. Lange, F. Camilo, N. Wex, M. Kramer, D. C. Backer, A. G. Lyne, and O. Doroshenko, *mnras* **326**, 274 (2001), arXiv:astro-ph/0102309.
- [23] J. Neyman and E. Pearson, *Philosophical Transactions of the Royal Society of London* **231**, 289 (1933).
- [24] A. C. Searle, ArXiv e-prints (2008), 0804.1161.
- [25] P. Jaranowski, A. Królak, and B. F. Schutz, *Phys. Rev. D* **58**, 063001 (1998), arXiv:gr-qc/9804014.
- [26] R. Wijnands, D. Altamirano, P. Soleri, N. Degenaar, N. Rea, P. Casella, A. Patruno, and M. Linares, eds., *A Decade of Accreting Millisecond X-Ray Pulsars*, vol. 1068 of *American Institute of Physics Conference Series* (2008).
- [27] R. Prix, *Phys. Rev. D* **75**, 023004 (2007), arXiv:gr-qc/0606088.
- [28] J. H. Conway and N. J. A. Sloane, *Sphere Packings, Lattices, and Groups* (New York: Springer-Verlag, 1993), second ed.
- [29] R. Prix, *Class. Quant. Grav.* **24**, S481 (2007).
- [30] C. Messenger, R. Prix, and M. A. Papa, *Phys. Rev. D* **79**, 104017 (2009), 0809.5223.
- [31] I. W. Harry, S. Fairhurst, and B. S. Sathyaprakash, *Class. Quant. Grav.* **25**, 184027 (2008).
- [32] S. Babak, *Class. Quant. Grav.* **25**, 195011 (2008).
- [33] G. M. Manca and M. Vallisneri, *Phys. Rev. D* **81**, 024004 (2010), 0909.0563.
- [34] G. M. Harry and the LIGO Scientific Collaboration, *Classical and Quantum Gravity* **27**, 084006 (2010).
- [35] B. P. Abbott, R. Abbott, R. Adhikari, P. Ajith, B. Allen, G. Allen, R. S. Amin, S. B. Anderson, W. G. Anderson, M. A. Arain, et al., *Phys. Rev. D* **80**, 042003 (2009), 0905.1705.